Title
Total Internal Reflection Fluorescence Microscopy.

Permalink
https://escholarship.org/uc/item/3kj6q6dt

Journal
Cold Spring Harbor Protocols, 2015(9)

ISSN
1940-3402

Authors
Yildiz, Ahmet
Vale, Ronald D

Publication Date
2015-09-01

DOI
10.1101/pdb.top086348

Peer reviewed

Total Internal Reflection Fluorescence Microscopy

Ahmet Yildiz and Ronald D. Vale

The goal in fluorescence microscopy is to detect the signal of fluorescently labeled molecules with great sensitivity and minimal background noise. In epifluorescence microscopy, it is difficult to observe weak signals along the optical axis, owing to the overpowering signal from the out-of-focus particles. Confocal microscopy uses a small pinhole to produce thin optical sections (∼500 nm), but the pinhole rejects some of the in-focus photons as well. Total internal reflection fluorescence microscopy (TIRFM) is a wide-field illumination technique that illuminates only the molecules near the glass coverslip. It has become widely used in biological imaging because it has a significantly reduced background and high temporal resolution capability. TIRFM has been used to study proteins in vitro as well as signaling cascades by hormones and neurotransmitters, intracellular cargo transport, actin dynamics near the plasma membrane, and focal adhesions in living cells. Because TIRF illumination is restricted to the glass–water interface and does not penetrate the specimen, it is well suited for studying the interaction of molecules within or near the cell membrane in living cells.

INTRODUCTION

Principles of Total Internal Reflection

Total internal reflection fluorescence microscopy (TIRFM) relies on the refraction and reflection of light from a planar surface. When the excitation beam travels from a high index of refraction medium ($n_1 = 1.518$ for glass) to a low index of refraction medium ($n_2 = 1.33$ for water), the angle of the beam changes in accordance with Snell's law. At a specific critical angle, the incident beam is totally reflected back from the glass surface, rather than passing through the water (Fig. 1). TIR is achieved when the incident angle is ∼2° higher than the critical angle (θ_c); $\sin(\theta_c) = n_2/n_1$, where $\theta_c = 61.5°$ for a glass–water interface.

In TIR, the reflected beam partially emerges from the glass and travels a subwavelength distance in water before returning back to the glass medium. Therefore, TIR generates a very thin electromagnetic field in the aqueous medium, which is called an evanescent field. The evanescent field decays exponentially with increasing distance from the glass–water boundary. The penetration depth (d) is a function of the wavelength (λ) and incident angle (θ) of the excitation beam and the refractive indices of the two media. The characteristic penetration depth is given by
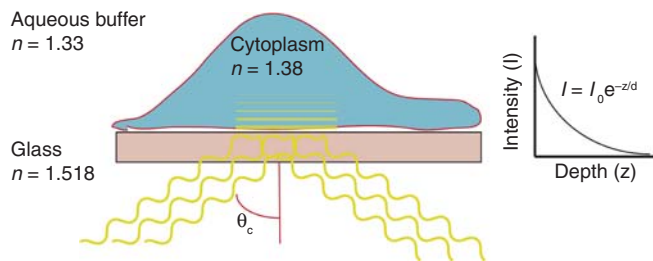
$$d = \frac{\lambda}{4\pi\sqrt{([n]_1 \sin\theta)^2 - n_2^2}}.$$

The penetration depth usually ranges between 80 and 200 nm for the visible spectrum and decreases as the incident angle grows larger. Beyond this distance, the electric field is insufficient to excite

Cite this introduction as *Cold Spring Harb Protoc*; doi:10.1101/pdb.top086348

A. Yildiz and R.D. Vale

FIGURE 1. Total internal reflection. The angle of the incident light above the critical angle is totally internally reflected back from the coverslip surface. The reflected beam generates an evanescent field that decays exponentially into the sample. TIR illuminates molecules near (∼100 nm) the glass surface. In live cell imaging, TIR only excites molecules in or near the cell membrane and significantly reduces background fluorescence.

fluorophores. Exponential decay of the evanescent wave intensity can be used to study the distance of molecules from the glass surface. In most live cell experiments, the TIRF interface is not as clearly defined as the glass–water boundary. The index of refraction of the cellular membrane ($n = 1.38$) is slightly higher than the aqueous medium, which results in higher penetration depth. Overall TIRFM generates a much thinner optical section and achieves better signal-to-noise ratio images than does confocal microscopy. However, because TIRF occurs only at the interface, it is not suitable for generating optical sections for three-dimensional imaging, as in the case of confocal microscopy. Daniel Axelrod has greatly stimulated the use of TIRFM for biological applications (Axelrod et al. 1984). Yanagida and co-workers have used the dramatic reduction in background fluorescence to image single molecules under TIRFM (Tokunaga et al. 1997).

Evanescent wave intensity at the surface is a function of the polarization of the incident beam. The plane of incidence is defined as the x–z plane. Two independent polarization directions (perpendicular [P] and parallel [S]) are possible with respect to the microscope's image plane (x–z plane). S-polarized light is perpendicular to the plane of incidence and generates polarization in the y-axis. P-polarized light remains in the plane of incidence and generates elliptical polarization in the x–z plane. Therefore, P-polarized light leads to slightly higher evanescent wave intensity with the same decay constant. To excite all possible orientations of fluorophores, it is suitable to introduce a quarter-wave plate into an optical pathway to generate a circularly polarized excitation beam.

Thin metallic layers are also used to enhance the fluorescence signal in TIRF. In these three-layer systems, light travels through glass, enters a metallic intermediate layer, and reflects back from the metal–water boundary. As the penetration depth changes in regard to the equations given above, the evanescent wave intensity at the surface is enhanced by surface plasmon resonance. This resonance is achieved through excitation of the surface plasmon mode of the metal, which increases the intensity of the signal by an order of magnitude. One interesting feature of metallic films is that they do not require a collimated beam for TIRF. Intensity is only enhanced for a narrow band of angles. Beams with higher or lower incident angles than the surface–plasmon angle produce only negligible fields. Thin films also lead to a highly P-polarized evanescent wave, regardless of the polarization angle of the incident beam. One consequence of a metallic coating is that particles closer than 10-nm proximity to the metal–water interface have their fluorescence quenched. To prevent fluorescence quenching, the surface of the metal can be coated with a transparent insulator material.

TIRFM Geometry

TIRFM can be achieved by two primary geometries that differ in their illumination pathways. In a prism-type TIRFM system, the laser beam is guided onto a surface through a prism to achieve the correct angle. In an objective-type TIRFM system, the laser beam travels through the objective before illuminating the sample. Figure 2 shows illumination pathways of both TIRFM types for an inverted microscope. A sample chamber is usually assembled from a clean coverslip and slide that have been attached together by double-sided tape. In the prism-type, the prism and slide are optically coupled
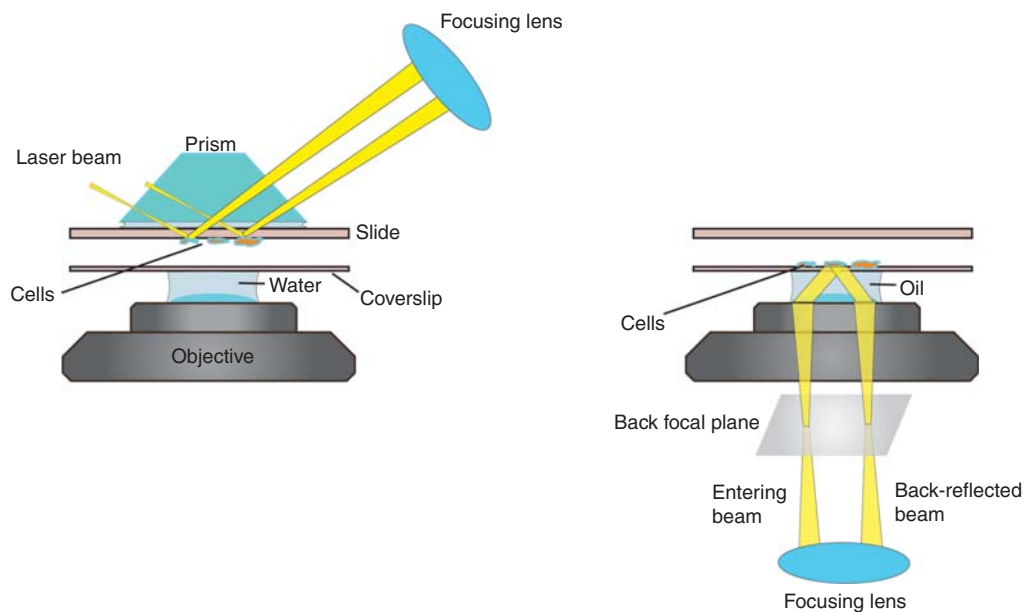
FIGURE 2. Geometries of TIRF illumination. (*Left*) In prism-type TIRF, the angle of incidence is adjusted by the focusing lens. Prism and quartz slide are optically coupled with matching immersion oil. TIR is generated on the surface of the slide and emitted photons are collected by a water-immersion objective through the coverslip. (*Right*) Using high-NA oil objectives, it is possible to guide the light through the sample above the critical angle to achieve TIR. The laser beam is focused to the objective back focal plane by a TIR lens. The lens is moved along the perpendicular axis to adjust the angle of incidence. Cells immobilized on a coverslip are illuminated by TIRF.

with immersion oil that matches their index of refraction. The angle of incidence is adjusted by moving the focusing lens via an *x–y–z*-translation stage. The size of illumination can be adjusted by the beam diameter and the focal length of the lens used (50- to 100-mm focal length lenses are commonly used). TIR is generated at the slide–water boundary and the fluorescence signal passes through aqueous medium, coverslip, and immersion medium to reach the objective. Because the excitation beam passes through a thick microscope slide, quartz slides and prisms are used to minimize autofluorescence. Light is collected by a high-numerical-aperture (NA = 1.3) water-immersion objective. To prevent the mismatch of refractive index owing to coverslip thickness, microscope companies provide adjustment collar for various coverslip thicknesses. Even though oil objectives can achieve higher NA, they suffer spherical aberration that is caused by the mismatch of the aqueous buffer and the immersion oil. The mismatch becomes negligible if the flow chamber is thinner than 15 µm and oil objectives can be used under these conditions.

Using high-NA objectives, it is possible to send the excitation beam through the objective below the critical angle for TIR. In this method, a collimated laser beam is focused onto the outer edge of the back focal plane of the microscope objective to obtain parallel beams exiting the objective's pupil with a high incidence angle. The need for a high-NA objective is illustrated by Snell's law, in which the critical angle is 61.5° for a glass–water interface (n_{water} = 1.33). A 1.4-NA oil-immersion objective makes it barely possible to achieve TIR. Recently, major microscope companies have begun to provide 1.45–1.49-NA oil-immersion objectives, resulting in a maximum illumination angle of 72°–75°. TIR alignment with these objectives is easier than with 1.4-NA objectives. Investment in a 1.45–1.49-NA objective is important for successful objective-type TIRFM.

Prism-type TIRF is easier to set up and provides more uniform illumination, which results in a lower background compared with the objective type. However, this method blocks the upper surface of the flow chamber, which is commonly used for buffer exchange, electrophysiology, and microinjection of the sample in life sciences. In addition, the prism has to be removed to exchange the sample, which necessitates realignment of the prism for each experiment. Even though objective-type TIRF leads to increased levels of light scattering within the objective, it is clearly the method of choice for

A. Yildiz and R.D. Vale

most laboratories. Because the emitted fluorescence travels through a coverslip, an objective collar readily corrects refractive index mismatch, and minimum spherical aberration is achieved.

TIRFM IMAGING SETUP

Most inverted microscopes can easily be converted into an objective-type TIRFM. Figure 3 shows the layout of an objective-type TIRFM system equipped with two lasers. To properly align a TIRFM system, do the following.

1. Adjust the two laser beams to the height of the microscope port using periscopes and combine them using a dichroic mirror placed on a kinematic mount. To ensure that the beams travel along the same optical path, use a set of two irises adjusted to the same height along the optical table.

2. Place a 5× beam expander on an *x*–*y*-translation stage along the optical pathway to obtain a large (∼60 μm diameter) illumination spot. If the two lasers have a significantly different beam diameter, then a combination of a 10× beam expander and an adjustable iris set at a 1-cm-diameter opening can be used to obtain the same illumination area for both lasers. To minimize chromatic aberrations in the beam expander, achromatic doublet lenses should be used.

3. (Optional) Send the beam to a kinematic mirror placed on a linear translation stage. The light reflects off at 90° at this mirror and is sent to the back illumination port of an inverted microscope.

4. Place an appropriate filter set in the filter turret of the microscope, and a circular field diaphragm onto the nosepiece. Adjust the mirror position to allow the center of the beam to coincide with the center of the object plane.

5. Place an achromatic doublet TIR lens with an *x*–*y*–*z*-translation stage along the optical path. The focal length of this lens determines the size of the illumination area, and can be 25–50 cm. First, adjust the lens position to allow the beam to pass through the center of the lens. Second, adjust its *z*-position to focus the laser beam to the center of the microscope nosepiece.
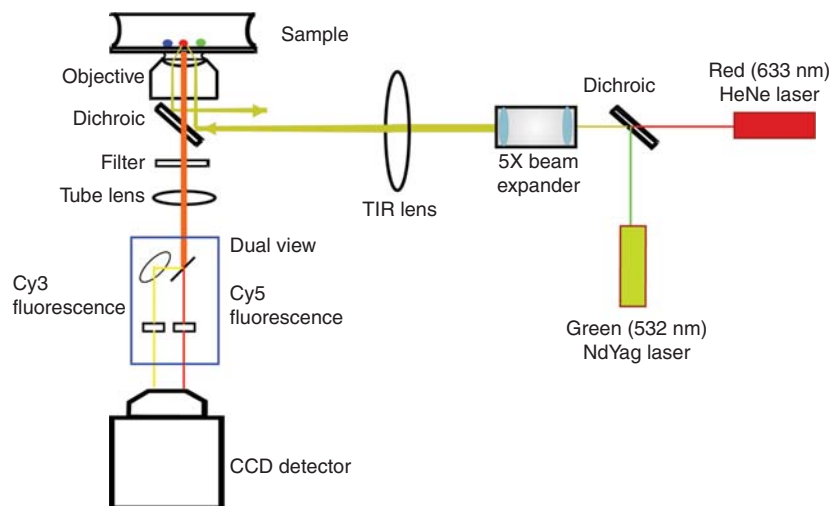
FIGURE 3. Schematics of a multicolor TIRFM. To simultaneously image Cy3 and Cy5 fluorescence, an objective-type TIRF microscope is equipped with 532- and 633-nm lasers. The laser beams are combined with a dichroic mirror and expanded through a Gaussian beam expander. The laser beams are focused onto the back focal plane of the microscope objective with an achromatic doublet lens (*f* = 500 mm). A set of multiband dichroic and emission filters are used to reflect the 532- and 633-nm laser beams onto the objective and to transmit Cy3 and Cy5 fluorescence simultaneously. The fluorescence is then separated by a Dual View instrument (Optical Insights Inc.), which is composed of a dichroic mirror to split Cy3 and Cy5 fluorescence, and band-pass emission filters to further reduce the cross talk between the two channels.

Cite this introduction as *Cold Spring Harb Protoc*; doi:10.1101/pdb.top086348

6. Remove the circular diaphragm from the nosepiece and place a high-NA (>1.4) objective lens. Readjust the x–y-position of the TIR lens to project the laser beam onto the ceiling, and the z-position to obtain smallest possible diameter of the laser beam. Because of the chromatic aberrations in most objectives, it is not possible to properly focus multiple laser beams simultaneously. Therefore, an intermediate position should be found or the z-position of the TIR lens should be adjusted before switching to another laser beam.

7. Add matching immersion oil to the objective. Prepare a flow chamber with surface immobilized fluorescent microspheres on a coverslip and place it on the microscope stage. Focus the objective lens on the sample by using binoculars to find the immobilized beads on the coverslip surface.

8. Adjust the x- or y-position of the TIR lens to move the focus spot within the back focal of the objective. The beam will be sent to the objective at off axis, which will tilt the direction of the beam at the objective exit pupil. When the critical angle is reached, parallel light traveling along the glass coverslip will be observed. Tilting the beam ∼2° more will generate TIR. A secondary spot corresponding to the back-reflected beam should be observed on a TIR lens along the direction of tilting.

9. Acquire images with a charge-coupled device (CCD) camera located on a plane conjugate to the object plane.

10. Adjustment of either the x- or y-position of the TIR lens may result in shifting the illumination area away from the center of the CCD chip. Readjust the x- or y-position of the 5× beam expander (or the mirror, if used) and then the TIR lens, until the center of the illumination area matches well with the center of the CCD chip.

EQUIPMENT

Light Sources

Noncoherent light sources are not recommended for TIRFM, because only a fraction of light exits the objective at higher angles than the critical angle. Argon-ion, krypton, and helium–neon are the common gas lasers used to excite the sample in the visible region of light. Recently, diode-pumped solid-state (DPSS) lasers have become popular owing to their small size, high stability, and low maintenance and power requirements. Major peaks of gas lasers (405, 488, 514, 532, 547, and 647 nm) are matched in commercial DPSS lasers to easily implement them into existing experimental setups. For multicolor TIRFM setups, different wavelength laser beams must be combined with the proper set of dichroic mirrors to attain collinear illumination. The laser beam can then be coupled to an optical fiber to purify nonuniform modes, and to obtain the same beam size for each laser beam. To perform single-molecule polarization assays in TIRFM, polarization-maintaining fibers should be used.

In multicolor time-lapse imaging assays, shuttering and changing the laser power may be required. DPSS lasers can be readily modulated by electronic signals at a megahertz frequency. Excitation of other lasers can be controlled in time series on a millisecond timescale by mechanical shutters. An acousto-optic tunable filter (AOTF) is also commonly used to rapidly (a few microseconds) modulate the transmission wavelength and intensity of the laser excitation. In AOTFs, there is a miniscule leakage of the blocked beams, which may lead to increased background noise. Therefore, in these systems, all possible laser wavelengths in the illumination pathway should be carefully blocked by respective emission filters to obtain a high signal-to-noise ratio.

In TIRFM, it is ideal to fully illuminate the field of view of the CCD cameras. Image magnification should fulfill the Nyquist criterion, which requires that the actual pixel size of the camera be less than half of the minimum resolvable distance (∼250 nm for visible light). Most camera companies provide CCD chips with 8–24-μm pixels. TIRF microscopes mostly use 100× objectives, and an additional 1.5× magnifier (built-in optivar in many commercial microscopes) can be used to meet this criterion if needed. We have found that the optimum pixel size of the CCD is between 80 and 160 nm for high

A. Yildiz and R.D. Vale

spatial resolution. Therefore, an ∼40–60 μm diameter circle (0.003 mm^2) should be illuminated with a laser light to fully illuminate a 512 × 512 camera chip. We have also found that 100–300 mW/mm^2 of laser power incident on the sample is sufficient to saturate most organic dyes. Therefore, 1 mW of incident beam on the sample is required to perform the measurements. TIRFM users should take into account the losses in the optical pathway before making a decision on which laser to purchase. In custom TIRFM setups, at least 50% of the light is lost in dichroic mirrors, lenses, filters, and the objective. In fiber optic-coupled systems, an additional 50%–70% of light is lost in the fiber couplers and the AOTF.

Filters

The proper choice of dichroic mirrors and emission filters can significantly improve the performance of the TIRFM system. Because the excitation beam is reflected back from the glass surface and travels back along the detection pathway, blocking the excitation beam is essential for detecting the fluorescence signal by a camera. Assuming that the excitation laser power is roughly a million times more powerful than the fluorescence signal, even miniscule leakage of the laser light into the detection pathway can dominate the signal. Because the entering beam is physically separated from the returning beam, two small mirrors can be used instead of a dichroic mirror to fully reflect the returning beam out of the fluorescence detection path.

For each set of fluorescent probes, a separate filter cube is assigned. The first step is to clean up the laser beam by using an excitation filter that has a narrow (∼10 nm) band pass. This step is required if the laser emits multiple wavelengths. Using an excitation filter also reduces the background even though the sample is illuminated with spectrally pure laser light. This is because excitation filters are designed based on the principles of thin-film interference at normal incident angles and they significantly block the off-axis light. In the absence of an excitation filter, a fraction of the off-axis light can pass through an emission filter and reach the camera chip.

The dichroic mirror should have the highest possible transmission for the entire emission spectrum of the fluorescent probe used, and reflection of the excitation wavelength. Because the emission spectrum often starts near the absorption maxima, a steep transition from reflection to transmission band is anticipated. Razor edge dichroic mirrors (Semrock) have been designed for most of the common excitation wavelengths to allow measurement of signals very close (2 nm) to the blocked laser light. Recent advances allow for ultrabright (up to 99% transmission), durable, and easy-to-clean dichroic mirrors that can be safely used at high laser powers without burning out. It is extremely important to ensure that the dichroic surface is flat in TIRFM. Any curvature leads to astigmatism in the beam profile, which would result in light entering the sample at various angles and increasing the background fluorescence. Bending of dichroic surfaces may be caused by differences in the intrinsic stress between the hard glass coatings and the substrate. In addition, overtightening the springs in the filter cube can easily bend the filter surface and cause higher-order aberrations. Care should be taken when assembling each filter cube.

For multipurpose TIRFM setups, we have often found it difficult to align the optical pathway for each dichroic mirror used in the microscope. Slight angular differences between dichroic mirrors shift the incident angle of the laser beam and change the location of the illumination area. For these purposes, we recommend a single multi-band-pass dichroic mirror that can block each excitation wavelength used in the setup and transmit the other wavelengths between them. With such mirrors, up to four lasers emitting at different wavelengths can be blocked by a single dichroic. Emission filters that match well with the spectrum of these dichroics can be used so that a single filter cube works for all combinations of excitation wavelengths and fluorescent dyes. This design significantly improves the temporal resolution of multicolor experiments, because it does not require rotating the filter wheel for each laser and eliminates the alignment problems caused by the tilt in the dichroic orientation.

Dichroic mirrors can only reflect 99% of the excitation light. The remaining light is blocked by the emission filter that can transmit down to ∼10^{-7} of the laser light. Current filters can achieve this performance even if the laser wavelength is only a few nanometers away from the transmission

band. Recently, transmission efficiency of these filters has been optimized to >95%, so that there are minimal losses within the detection pathway. Long-pass emission filters can be used to detect a red-shifted tail of the fluorescence emission for bright samples. However, at low-light levels, Raman scattering of water can become significant and band-pass emission filters are recommended to block this background noise. The Raman peak is red-shifted to the excitation wavelength by 3400 cm^{-1} for pure water. For example, excitation of a Cy3- or rhodamine-stained sample with a 532-nm laser line results in Raman scattering at 649 nm. Using a band-pass filter that collects fluorescence emission between 540 and 620 nm is likely to provide the highest signal to noise.

Objectives

To achieve TIR, a specimen must be illuminated with a numerical aperture greater than the refraction index of the media ($n = 1.38$ for cells). It is therefore possible to use 1.4-NA oil-immersion objectives, but only a very small fraction (0.02) of the lens numerical aperture can be used. Major microscope vendors now offer up to 1.49 NA for oil-immersion objectives that can send the beam to the sample at higher incidence angles. Alignment of TIR with these objectives is therefore much easier. We use Plan Apochromatic objective lenses in TIRFM because they are well corrected for chromatic aberration and for flatness of field, resulting in high-quality images.

Olympus also offers a 100× 1.65-NA oil Apochromatic objective to achieve a very steep angle in illumination. Increasing the angle of incidence generates a thinner evanescent field and further reduces the background. The high NA of the objective also increases the resolving power of the microscope, which is limited by the diffraction limit ($\lambda/2$ NA) of light. However, this objective requires a sapphire coverslip ($n = 1.78$) with matching volatile immersion liquid, a costly and impractical solution for everyday usage. The 1.65-NA objective is usually used only for very weak signals.

Fluorescence Detection and Image Acquisition

Because TIRFM is a wide-field illumination technique, the image of the object is formed on the surface of a camera. CCD cameras are used in TIRFM to detect the fluorescence signal. Image acquisition speed of the camera, which is a function of camera readout rate and pixel size, should be compatible with the dynamics of the biological system under study. For example, tracking the diffusion of transmembrane proteins, which is on the order of 1 μm^2/sec, requires a millisecond temporal resolution. High acquisition speeds can be achieved by either selecting a small region of interest or by increasing the readout rate of the camera. For weak signals (i.e., single-particle tracking), the system noise is mainly determined by the readout noise of the camera. Intensified CCD cameras are used to multiply the incoming photons before they reach the CCD chip. Therefore, the effect of the readout noise is minimized. However, the image intensifier causes a spread of photons to neighboring pixels, which results in wider point spread functions and blurry images. Although intensified CCDs can achieve high gain and fast acquisition speeds, they are relatively expensive and susceptible to photodamage.

Electron-multiplying (EM) CCD cameras now dominate the market for imaging weak signals. In an EMCCD, photons are multiplied after they reach the chip by an on-chip gain registry. By applying high clock voltages, secondary electrons can be obtained by a process called impact ionization. Even though this process is stochastic and probability of secondary electron generation is low (0.013), transferring the charges in CCD registry multiple times can achieve a 1000-fold gain in the signal. Therefore, EMCCDs are capable of detecting single photon events by eliminating the readout noise of the output amplifier. However, the stochastic nature of the impact ionization process adds an uncertainty to the number of counts per pixel. This is called an *excess noise factor*, which multiplies photon shot noise by 1.4. The high clock voltages may also produce a secondary electron even when no primary electron is present for transfer. Therefore, the current state of EM is beneficial for low-light-level imaging. At higher signals, excess noise factors in EM registry reduce the signal-to-noise ratio. Andor Technology, Hamamatsu, Roper Scientific, and QImaging offer various chip sizes of these cameras, which can also be operated as a conventional CCD for high signal levels. By using back-

illuminated chip design, 92% of the incoming photons can be detected in the visible region of light. To perform photon acquisition and readout simultaneously, interline or frame-transfer chip design are commonly used. In short, these cameras can detect the signal from single fluorophores with high sensitivity by generating minimal detection noise. Currently, 2-msec temporal resolution can be achieved with 10-MHz readout of a small-chip (128×128) EMCCD. New cameras with higher readout rates and lower excess noise factors are anticipated in the near future.

Commercial TIRF Systems

Objective-type TIRFM setups have been commercialized recently by major microscope vendors (Agilent Technologies, Leica, Nikon, Carl Zeiss, and Olympus). Commercial TIRFM systems are equipped with multiple laser sources coupled to an optical fiber and controlled through an AOTF. The fiber is collimated in front of a TIRF illuminator that consists of a focusing lens and a motorized x–y–z stage to adjust the illumination angle. The illuminator spreads out the light over the full field of view within the binoculars and minimizes the amount of scattered light from the objective. High power lasers are recommended for commercial systems, because a large portion of light (50%) is lost through the fiber coupling, and increasing the field of view decreases the laser power per area. These systems are easier to use and do not require much experience with optics to align them. Many cell biology laboratories have started to use commercial systems for live cell imaging applications.

TIRFM APPLICATIONS

TIRFM is well suited for studying single-molecule dynamics for time-resolution demanding applications. Early studies were performed on purified proteins immobilized onto a glass coverslip. In the initial reports of TIRFM for single-molecule imaging, Funatsu et al. (1995) showed binding and dissociation of fluorescently labeled nucleotides to single myosin motors. By monitoring the intensities of diffraction limited spots corresponding to single molecules, diffusional movement of rhodamine-labeled membrane proteins was observed within a lipid bilayer (Schmidt et al. 1996). The TIRFM pathway can be modified to perform fluorescence polarization or fluorescence resonance energy transfer assays to measure conformational changes of motors in vitro (Sosa et al. 2001; Mori et al. 2007). In addition, superior image quality and high temporal resolution of TIRFM allow for high-precision tracking of the diffraction-limited image of single molecules. The center of the fluorescent spot is localized within 1 nm precision using a Gaussian algorithm to study the movement of motor proteins (Yildiz et al. 2003).

TIRFM provides a significant advantage for exploring protein dynamics on a plasma membrane in live cells. The evanescent field eliminates the high autofluorescence of the cytoplasm and allows tracking of individual membrane proteins. By measuring the intensity and the diffusion constant of GFP-tagged membrane proteins, cluster formation of focal-adhesion molecules (Iino et al. 2001), ion channels (Harms et al. 2001), and anchoring proteins (Murakoshi et al. 2004) has been shown experimentally. Our laboratory has used glass-adsorbed lipid bilayers to introduce immune recognition proteins found in antigen-presenting cells (e.g., integrins, such as ICAM1) to T cells. As first shown by Dustin and colleagues, these bilayers can mimic the antigen-presenting cells and create a complex signaling structure called the "immunological synapse" (Grakoui et al. 1999). Using multicolor TIRFM, we have imaged fluorescently labeled proteins on the bilayer and the T-cell membrane simultaneously, and have observed the formation of a microdomain of signaling proteins during T-cell signaling (Fig. 4) (Douglass and Vale 2005).

Cellular components close to the membrane also can be observed by TIRF, because the characteristic depth of the evanescent wave is higher in live cells. We have used multicolor TIRFM to image myosin and microtubules at the cortex during the process of cytokinesis (Fig. 5) (Vale et al. 2009). To facilitate the use of TIRFM for such applications, cells can be spread and flattened on the coverslip by using adhesion molecules (e.g., concanavalin A).
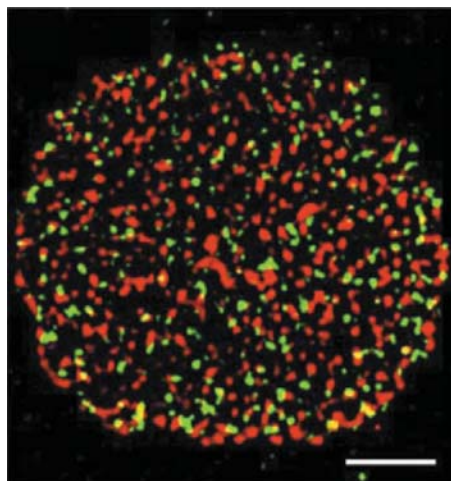
FIGURE 4. Multicolor tracking of single molecules in a T-cell membrane. Superimposed images of single molecules of green fluorescent protein (GFP)-tagged Lck kinase (green) and a confocal image (multiple molecules imaged) of the membrane receptor CD2 (red) in Jurkat T cells. Diffusion of individual kinase molecules was tracked relative to CD2-containing microdomains by TIRFM. Scale bar, 5 µm. (Reprinted from Douglass and Vale 2005.)

Recent advances in TIRFM imaging have made a huge impact in understanding the mechanism and function of cellular components including membrane proteins, signaling cascades, and molecular motors. The relative ease of alignment and use of TIRF combined with high sensitivity in single-molecule detection makes it an extremely powerful technique to tackle a wide array of cellular questions. The availability of the commercial systems is now allowing much wider applications of TIRFM in cell biology laboratories. The principles of TIRFM are illustrated in our accompanying protocol, **Tracking Movements of the Microtubule Motors Kinesin and Dynein Using Total Internal Reflection Fluorescence Microscopy** (Yildiz and Vale 2015).
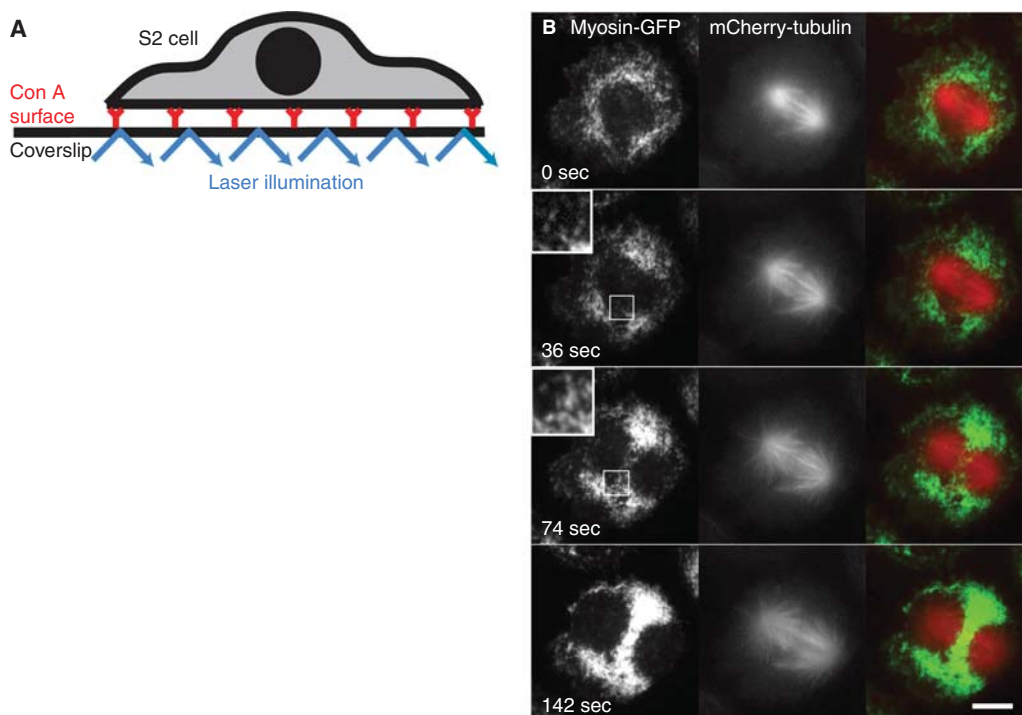
FIGURE 5. TIRFM imaging of myosin proteins during cell division. (*A*) *Drosophila* S2 cells were spread over a concanavalin A-coated glass surface and imaged under TIRFM. (*B*) Sequence of TIRFM images of GFP-myosin (*left*) superimposed onto wide-field images of mCherry-tubulin (*right*) shows the redistribution of myosin during anaphase. Scale bar, 10 µm. (Reprinted from Vale et al. 2009.)

Cite this introduction as *Cold Spring Harb Protoc*; doi:10.1101/pdb.top086348

A. Yildiz and R.D. Vale

ACKNOWLEDGMENTS

REFERENCES

Axelrod D, Burghardt TP, Thompson NL. 1984. Total internal reflection fluorescence. *Annu Rev Biophys Bioeng* **13:** 247–268.

Douglass AD, Vale RD. 2005. Single-molecule microscopy reveals plasma membrane microdomains created by protein–protein networks that exclude or trap signaling molecules in T cells. *Cell* **121:** 937–950.

Funatsu T, Harada Y, Tokunaga M, Saito K, Yanagida T. 1995. Imaging of single fluorescent molecules and individual ATP turnovers by single myosin molecules in aqueous solution. *Nature* **374:** 555–559.

Grakoui A, Bromley SK, Sumen C, Davis MM, Shaw AS, Allen PM, Dustin ML. 1999. The immunological synapse: A molecular machine controlling T cell activation. *Science* **285:** 221–227.

Harms GS, Cognet L, Lommerse PH, Blab GA, Kahr H, Gamsjäger R, Spaink HP, Soldatov NM, Romanin C, Schmidt T. 2001. Single-molecule imaging of l-type Ca^{2+} channels in live cells. *Biophys J* **81:** 2639–2646.

Iino R, Koyama I, Kusumi A. 2001. Single molecule imaging of green fluorescent proteins in living cells: E-cadherin forms oligomers on the free cell surface. *Biophys J* **80:** 2667–2677.

Mori T, Vale RD, Tomishige M. 2007. How kinesin waits between steps. *Nature* **450:** 750–754.

Murakoshi H, Iino R, Kobayashi T, Fujiwara T, Ohshima C, Yoshimura A, Kusumi A. 2004. Single-molecule imaging analysis of Ras activation in living cells. *Proc Natl Acad Sci* **101:** 317–322.

Schmidt T, Schütz GJ, Baumgartner W, Gruber HJ, Schindler H. 1996. Imaging of single molecule diffusion. *Proc Natl Acad Sci* **93:** 2926–2929.

Sosa H, Peterman EJ, Moerner WE, Goldstein LS. 2001. ADP-induced rocking of the kinesin motor domain revealed by single-molecule fluorescence polarization microscopy. *Nat Struct Biol* **8:** 540–544.

Tokunaga M, Kitamura K, Saito K, Iwane AH, Yanagida T. 1997. Single molecule imaging of fluorophores and enzymatic reactions achieved by objective-type total internal reflection fluorescence microscopy. *Biochem Biophys Res Commun* **235:** 47–53.

Vale RD, Spudich JA, Griffis ER. 2009. Dynamics of myosin, microtubules, and Kinesin-6 at the cortex during cytokinesis in *Drosophila* S2 cells. *J Cell Biol* **186:** 727–738.

Yildiz A, Vale RD. 2015. Tracking movements of the microtubule motors kinesin and dynein using total internal reflection fluorescence microscopy. *Cold Spring Harb Protoc* doi: 10.1101/pdb.prot086355.

Yildiz A, Forkey JN, McKinney SA, Ha T, Goldman YE, Selvin PR. 2003. Myosin V walks hand-over-hand: Single fluorophore imaging with 1.5-nm localization. *Science* **300:** 2061–2065.

Cite this introduction as *Cold Spring Harb Protoc;* doi:10.1101/pdb.top086348

Total Internal Reflection Fluorescence Microscopy

Ahmet Yildiz and Ronald D. Vale

Email Alerting Service	Receive free email alerts when new articles cite this article - **click here.**
Subject Categories	Browse articles on similar topics from *Cold Spring Harbor Protocols.* Cell Biology, general (1228 articles) Cell Imaging (504 articles) Fluorescence (482 articles) Fluorescent Proteins (246 articles) Image Analysis (114 articles) Imaging/Microscopy, general (566 articles) Live Cell Imaging (265 articles) Visualization (496 articles) Visualization of Proteins (100 articles)